

Extracting cosmic microwave background polarisation from satellite astrophysical maps

C. Baccigalupi^{1,2}, F. Perrotta^{2,3}, G. De Zotti³, G.F. Smoot², C. Burigana⁴,
 D. Maino^{5,6}, L. Bedini⁷, E. Salerno⁷

¹ SISSA/ISAS, Astrophysics Sector, Via Beirut, 4, I-34014 Trieste, Italy

² Lawrence Berkeley National Laboratory, 1 Cyclotron Road, Berkeley, CA 94720, USA

³ INAF, Osservatorio Astronomico di Padova, Vicolo dell’Osservatorio 5, I-35122 Padova, Italy

⁴ ITeSRE-CNR, Via Gobetti, 101, I-40129 Bologna, Italy

⁵ INAF, Osservatorio Astronomico di Trieste, Via G.B. Tiepolo, 11, I-34131 Trieste

⁶ Dipartimento di Fisica, Università di Milano, Via Celoria 16, I-20133, Italy

⁷ IEI-CNR, Via Moruzzi 1, I-56124 Pisa, Italy

2 December 2024

ABSTRACT

We present the application of the Fast Independent Component Analysis (FASTICA) technique for blind component separation to polarised astrophysical emission. We study how the Cosmic Microwave Background (CMB) polarised signal, consisting of *E* and *B* modes, can be extracted from maps affected by substantial contamination from diffuse Galactic foregrounds and instrumental noise.

We perform the analysis of all sky maps simulated accordingly to the nominal performances of the Low Frequency Instrument (LFI) aboard the PLANCK satellite; the sky signal is modeled as a superposition of CMB, generated by a Gaussian, nearly scale invariant cosmological perturbation spectrum, and the existing simulated polarisation templates of Galactic synchrotron. Our results indicate that the angular power spectrum of CMB *E* modes can be recovered on all scales up to $\ell \simeq 1000$, corresponding to the fourth acoustic oscillation, while *B* modes can be detected, up to their turnover at $\ell \simeq 100$ if cosmological tensor amplitude exceeds a 30% fraction of scalar perturbations. Moreover, we assess the instrumental capability to recover the cross correlation between total intensity and polarisation, *TE*, recovering the spectrum up to $\ell \simeq 1200$, corresponding to the seventh *TE* acoustic oscillation.

For comparison, we study the performance of the Microwave Anisotropy Probe (MAP) satellite for polarised radiation and in presence of foregrounds; we find CMB polarisation detection in the interval $100 \leq \ell \leq 500$ for *TE*, corresponding to the first three acoustic oscillations, and a marginal detection of the peak of the second *E* mode acoustic oscillation, in the interval $300 \leq \ell \leq 400$.

Key words: methods – data analysis – techniques: image processing – cosmic microwave background.

1 INTRODUCTION

Observations of the Cosmic Microwave Background (CMB) anisotropies undergo an enormous progress in this decade. After the first evidence of CMB total intensity fluctuations as measured by the COsmic Background Explorer (COBE) satellite (see Smoot 1999 and references therein), several balloon-borne and ground-based operating experiments were successful in detecting CMB anisotropies on degree and sub-degree angular scales (De Bernardis et al 2002, Halverson et al. 2002, Lee et al. 2001, Padin et al. 2001). The Microwave Anisotropy Probe (MAP) satellite (Wright 1999, see also <http://map.gsfc.nasa.gov/>)

2 *Baccigalupi et al.*

is presently operating and will provide in approximately one year a full sky map of the CMB anisotropies with about 14 arcminutes resolution and a sensitivity of the order of a few tens of μK , on a frequency range extending from 22 to 90 GHz. The experimental effort toward a definitive all sky measure of CMB anisotropies will culminate with the observations produced by the PLANCK satellite, scheduled for launch in 2007 (Mandolesi et al. 1998, Puget et al. 1998, see also <http://astro.estec.esa.nl/SA-general/Projects/Planck>), providing total intensity and polarisation full sky maps of CMB anisotropy with resolution $\gtrsim 5'$ and a sensitivity of a few μK , on nine frequency in the frequency range 30-857 GHz.

Correspondingly to these experimental efforts, data analysis science faces entirely new and challenging issues to handle the amount of incoming data, and to extract all the relevant physical information about the cosmological signal and the other astrophysical emissions, coming from extra-Galactic sources as well as from our own Galaxy itself.

The latter aspect is closely related to the subject of the present work. As we already mentioned, the satellites MAP and PLANCK perform observations on 5 and 9 frequency channels, in the ranges 22-90 GHz and 30-857 GHz, respectively. On such a huge frequency range, several astrophysical processes will be observed, in addition to the CMB. For what concerns our own Galaxy, on frequencies below 100 GHz, the main foreground is expected by synchrotron (see Haslam et al. 1982 for an all sky template at 408 MHz) and free-free (traced by $\text{H}\alpha$ emission, see Haffner, Reynolds, Tufte 1999 and references therein); on higher frequencies, Galactic emission is expected to be dominated by thermal dust (Schlegel, Finkbeiner, Davies 1998), even if it is expected to appear even below 100 GHz, at low Galactic latitudes. Moreover, several populations of extra-Galactic sources, with different spectral behavior, are expected on all the frequencies (see Toffolatti et al. 1998), including the Sunyaev-Zel'Dovich effect from clusters of galaxies (Moscardini et al. 2002). Since astrophysical emission mechanisms have generally different frequency dependences, it is conceivable to combine suitably multi-frequency maps in order to recover a template for each emission process singularly.

A lot of work has been recently dedicated to provide algorithms devoted to the component separation task, exploiting different ideas and tools from signal processing science. Such algorithms generally deal separately with point-like objects like extra-Galactic sources (Tenorio et al. 1999, Vielva et al. 2001), and diffuse emissions from our own Galaxy. In this work we focus on techniques developed to handle diffuse emissions; such techniques can be broadly classified in two main categories. The “non-blind” approach consists in assuming priors on the signals to recover, on their spatial pattern and frequency scalings, in order to regularize the inverse filtering going from the noisy, multi-frequency data to the separated components: Wiener filtering (WF, Tegmark, Efstathiou 1996, Bouchet, Prunet, Sethi 1999) and Maximum Entropy Method (MEM, Hobson et al. 1998) have been tested with good results, even if applied to the whole sphere (Stolyarov et al. 2002). Part of the priors can be obtained from complementary observations, and the remaining ones have to be assumed.

The “blind” approach consists instead in performing separation by only assuming the statistical independence of the signals to recover, without priors neither on their frequency scalings, nor on their spatial statistics. This is possible by means of a novel technique in signal processing science, the Independent Component Analysis (ICA, see Amari S., Chichocki 1998 and references therein). The first astrophysical application of this technique (Baccigalupi et al. 2000) exploited an adaptive (i.e. capable of self-adjusting on time streams with varying signals) ICA algorithm, working successfully on limited sky patches for ideal noiseless data. Maino et al. (2002) implemented a fast, non-adaptive version of such algorithm (FASTICA, see Hyvärinen 1999) which was successful in reaching separation of CMB and foregrounds on several combinations of simulated all sky maps in conditions corresponding to the nominal performances of PLANCK, for total intensity measurements. Blind techniques for component separation are expected to be useful as the only possible approach when foreground contamination is poorly known, as well as an independent check on the results of a non-blind separation procedure.

In this work we apply the FASTICA technique to astrophysical polarised emission. CMB polarisation is expected to arise from Thomson scattering of photons and baryons at decoupling. Due to its tensor nature, physical information is coded in a entirely different way with respect to total intensity. Cosmological perturbations may be divided into scalars, like density perturbations, vectors, for example vorticity, and tensors, i.e. gravitational waves (see Kodama & Sasaki 1984). Total intensity CMB anisotropies simply sum up contributions from all kinds of cosmological perturbations. For polarisation, two non-local combinations of the Stokes parameters Q and U can be built, commonly known as E and B modes (see Zaldarriaga, Seljak 1997 and Kamionkowski, Kosowsky, Stebbins 1997 featuring a different notation, namely gradient G for E and curl C for B). It can be shown that the E component sums up the contributions from all the three kinds of cosmological perturbations mentioned above, while the B modes are excited via vectors and tensors only. Also, scalar modes of total intensity, which we label with T in the following, are expected to be strongly correlated with E modes: indeed, the latter are merely excited by the quadrupole of density perturbations, coded in the total intensity of CMB photons, as seen from the rest frame of charged particles at last scattering (see Hu et al. 1999 and references therein); therefore, for CMB, the correlation TE between T and E modes is expected to be the strongest contribution from polarisation.

This phenomenology is clearly much richer with respect to total intensity, and motivated a great interest toward CMB polarisation, not only as a new data set in addition to total intensity, but as the best potential carrier of cosmological information via electromagnetic waves. Unfortunately, as we describe in the next Section, polarised foregrounds are even less known in polarisation than in total intensity, see De Zotti (2002) and references therein for reviews. For this reason, it

is likely that a blind technique will be required to clean CMB polarisation from contaminating foregrounds. The first goal of this work is to present a first implementation of the existing ICA techniques on polarised astrophysical maps. Second, we want to assess the precision with which CMB polarised emission will be measured in the near future: we exploit the FASTICA technique on frequency below 100 GHz where some foreground model have been carried out (Giardino et al. 2002, Baccigalupi et al. 2001), adopting the nominal instrumental performances of the Low Frequency Instrument (LFI) aboard PLANCK (see <http://astro.estec.esa.nl/SA-general/Projects/Planck>). We also provide a comparison of the results with what is achievable adopting the MAP nominal features (see <http://map.gsfc.nasa.gov/>).

The paper is organized as follows. In Section 2 we describe how the simulation of the synchrotron emission were obtained. In Section 3 we describe our approach to component separation for polarised radiation. In Section 4 we study the FASTICA performance on our simulated sky maps. Section 5 we apply our technique to the PLANCK-LFI, quantifying its capability in polarisation measurements, and providing a comparison with the expected performance by MAP. Finally, Section 6 contains the concluding remarks.

2 SIMULATED POLARISATION MAPS AT MICROWAVE FREQUENCIES

As the background cosmology, we assume a flat Friedmann Robertson Walker (FRW) metric with Hubble parameter today $H_0 = 100h$ km/sec/Mpc with $h = 0.7$. The Cosmological Constant represents 70% of the critical density today, $\Omega_\Lambda = 0.7$, while the energy density in baryons is given by $\Omega_b h^2 = 0.022$; the remaining fraction is in Cold Dark Matter (CDM); we allow for a reionisation with optical depth to the reionisation last scattering $\tau = 0.05$, which can be seen as an upper limit in view of the recent evidences of reionisation occurring not much above redshift 6 (Becker et al. 2001). Cosmological perturbations are Gaussian, with spectral index for the scalar component leading to a not perfectly scale invariant spectrum, $n_S = 0.96$, and including tensor perturbations giving rise to B modes in the CMB power spectrum; we assume a ratio $R = 30\%$ between tensor and scalar amplitudes, and the tensor spectral index is taken to be $n_T = -R/6.8$ according to the simplest models of the very early Universe (see Liddle & Lyth 2000 and references therein). The cosmological parameters leading to our CMB template can be summarized as follows:

$$h = 0.7, \Omega_\Lambda = 0.7, \Omega_b h^2 = 0.022, \Omega_{CDM} = 1 - \Omega_\Lambda - \Omega_b, \tau = 0.05, n_S = 0.96, R = 0.3, n_T = -R/6.8. \quad (1)$$

We simulate whole sky maps of Q and U out of the theoretical C_ℓ^E and C_ℓ^B coefficients as generated by CMBFAST (Seljak & Zaldarriaga 1996), in the HEALPix environment (Górski et al. 1999); the maps are in antenna temperature, which is obtained at any frequency ν multiplying the thermodynamical fluctuations by a factor $x^2 \exp x / (\exp x - 1)^2$, where $x = h\nu/kT_{CMB}$, h, k are the Planck and Boltzmann constant, respectively, while $T_{CMB} = 2.726$ K is the CMB thermodynamical temperature.

Polarised emission from diffuse Galactic foregrounds in the frequency range which will be covered by the PLANCK satellite are very poorly known. On the high frequency side, $\nu \gtrsim 100$ GHz, the Galactic contribution to the polarised signal should be dominated by dust emission, which is still poorly known and for this reason under deep study (Lazarian & Prunet 2002). On the low frequency side, $\nu \lesssim 100$ GHz, the emission is expected to be dominated by the Galactic synchrotron, and several observations in the radio band actually exist, covering about half of the sky at the degree resolution (Brouw & Spoelstra 1976), as well as low and medium Galactic latitudes with 10 arcminutes resolution (Duncan et al. 1997, Uyaniker et al. 1999, Duncan et al. 1999). These data allow an estimate of the polarised synchrotron emission, and in particular of its angular power spectrum, down to scales as small as 10 arcminutes (Tucci et al. 2000, Baccigalupi et al. 2001, Giardino et al. 2002; in a recent work, Tucci et al. 2002 were able to probe arcminutes angular scales). A remarkable conclusion, arising from the present knowledge of the polarised backgrounds, is that CMB B modes are likely to be subdominating with respect to the foreground contribution at any frequency (Baccigalupi et al. 2002b, Lazarian & Prunet 2002). Indeed, at least in the cosmological scenarios we are assuming here, the CMB B modes get contribution from tensor perturbations (see Liddle & Lyth 2000 for reviews), which are subdominant with respect to the scalar component according to the recent estimates (Baccigalupi et al. 2002a); in addition, tensor perturbations vanish as radiation on sub-degree angular scales, corresponding to sub-horizon angular scales at decoupling; even if some power could be introduced by weak lensing phenomena occurring along the line of sight (see Hu 2002 and references therein) the cosmological B power is always expected to be much lower than the expected one for E modes. On the other hand, the Galaxy is likely to have approximately the same power in E and B modes (Zaldarriaga 2001), expected to be higher than cosmological B modes at frequency (Baccigalupi et al. 2002b, Lazarian & Prunet 2002).

Baccigalupi et al. (2001) estimated the power spectrum of synchrotron as derived by two main datasets. As we already mentioned, on super-degree angular scales, corresponding to multipoles $\ell < 200$, the foreground contamination is determined according to the Brouw & Spoelstra (1976) data, covering roughly half of the sky with degree resolution. The C_ℓ behavior on smaller angular scales has been obtained analyzing more recent data reaching a resolution of about 10 arcminutes (Duncan et al. 1997, 1999, Uyaniker et al. 1999). These data, extending in longitude for a relevant fraction of the Galactic plane and reaching Galactic latitudes up to $b \simeq 20^\circ$, are characterized by a flatter slope, $C_\ell \simeq \ell^{-(1.5 \pm 1.8)}$. Fosalba et al. (2002) interestingly provided evidence of a similar slope for the angular power spectrum of the polarisation degree induced by the

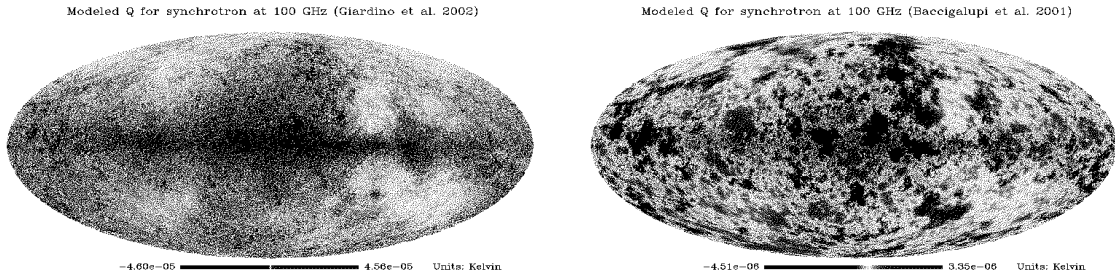


Figure 1. Q Stokes parameter for the emission of Galactic synchrotron according to Giardino et al. (2002, left panel) and Baccigalupi et al. (2001, right panel). The maps are in antenna temperature, at 100 GHz.

Galactic magnetic field as measured from starlight data. The synchrotron spectrum at higher frequencies, up to 100 GHz, was then inferred by scaling the one obtained in the radio band with a typical synchrotron spectral index -2.9 (antenna temperature).

Giardino et al. (2002) also found the slope of the synchrotron angular power spectrum in the radio band in agreement with Baccigalupi et al. (2001) and Tucci et al. (2000). Giardino et al. (2002) built a full sky map of synchrotron polarised emission derived by the total intensity map as measured by Haslam et al. (1982), assuming a synchrotron polarised component at the theoretical level of 75%, and a random polarisation angle; since the Haslam map has a resolution of about one degree, on smaller angular scales they assumed a power with a slope according to the data in the radio band but amplitude considerably higher, to match the power derived from the Haslam map. The polarisation map obtained, reaching a resolution of about ten arcminutes, were then scaled at higher frequencies by considering either constant or a space-varying spectral index as inferred by multi-frequency radio observations.

The knowledge of the polarised foreground emission is far from being satisfactory; however, synchrotron is expected to be the dominant polarised foreground at frequencies covered by MAP and by the Low Frequency Instrument (LFI) aboard the PLANCK satellite, extending from 22 to 100 GHz, even if some evidence of spinning or magnetized low frequency dust emission exists (Lazarian & Prunet 2002). Therefore in this work we concentrate on these frequencies, modeling the diffuse emission as a superposition of CMB and synchrotron. We adopted the synchrotron spatial template by Giardino et al. (2002), hereafter S_G model; we also consider another synchrotron template, hereafter indicated as S_B , obtained by rescaling the spherical harmonics coefficients amplitude of the S_G model to match the spectrum found by Baccigalupi et al. (2001): the Q Stokes parameter for the two spatial templates, in antenna temperature at 100 GHz, are shown in Fig. 1, plotted in a non-linear scale to highlight the behavior at high Galactic latitudes. Note how the contribution on smaller angular scales is larger in the S_G model; this is quantitatively evident in Fig. 2 where we report the power spectra of the S_G and S_B models compared to the CMB one as resulting from (1). Both models imply a severe contamination of the CMB E modes on large angular scales, say $\ell \lesssim 200$, even at 100 GHz frequencies, which remains serious even if the Galactic plane is cut out. In the S_G case the contamination is severe also for the first CMB acoustic oscillation in polarisation, as a result of the enhanced power on small angular scales with respect to the S_B models which is also evident in Fig. 1. On smaller scales, when comparing with CMB, both models predict the dominance of CMB E modes. On the other hand, CMB B modes are dominated by foreground emission.

To obtain the synchrotron emission at different frequencies, we consider either a constant -2.9 as well as a varying spectral index. In Fig. 3 we show the map of synchrotron spectral index, in antenna temperature, which we adopt as in Giardino et al. (2002). Note that this aspect is relevant especially for component separation, since all methods developed so far require a “rigid” frequency scaling of all the components, which means that all components should have separable dependence on space and frequency. Actually this requirement is hard to be satisfied for real signals, and for synchrotron in particular. However, as we see in the next Section, FASTICA reveals to be quite stable on the relaxation of this assumption, at least for the level of variation in Fig. 3. The stability of the algorithms developed so far for component separation against relaxation of the most severe assumptions about signals as well as instrument systematics is a crucial test to establish to what extend such algorithms can be applied to real data. From this point of view, the stability we found for relaxation of the rigid scaling assumption mentioned above, is a promising feature of the present technique. A more quantitative analysis of the FASTICA stability against space-varying spectral index, as well as most important sources of systematics for a given instrument, will be carried out in a forthcoming work.

Summarizing, in this paper we consider both the S_G and S_B models as Galactic foreground emission to be removed through component separation. The High Frequency Instrument (HFI) aboard PLANCK is also sensitive to polarisation; however, as

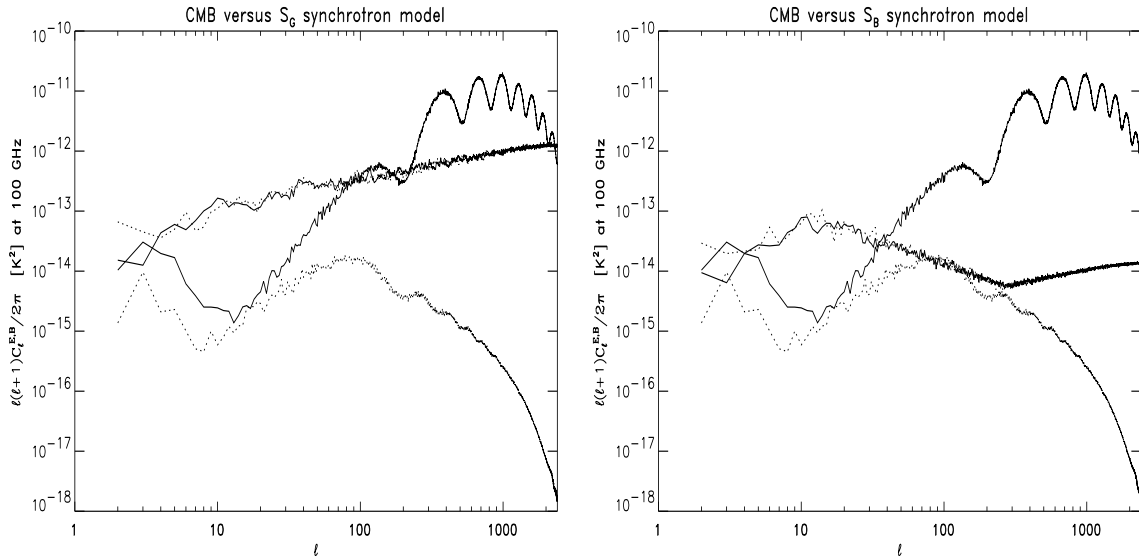


Figure 2. E (solid) and B (dotted) angular power spectra of CMB and synchrotron polarisation emission, in antenna temperature, at 100 GHz, according to the synchrotron model by Giardino et al. (2002), left panel, and Baccigalupi et al. (2001), right panel.

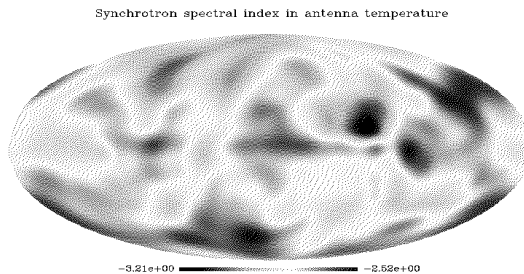


Figure 3. Map of synchrotron spectral index as reported in Giardino et al. (2002).

we stressed above, the polarised contamination at those frequencies is still under deep study, and no simulated templates of the foreground emission are available; for this reason we consider here only the lower frequency case, $\nu \lesssim 100$ GHz.

3 COMPONENT SEPARATION FOR POLARISATION RADIATION

Component separation has been implemented so far for the total intensity signal (see Maino et al. 2002, Stolyarov et al. 2002, and references therein). In this Section we expose how we extend the ICA technique to treat polarisation measurements.

3.1 E and B modes

The Stokes parameters Q and U are measured experimentally for linearly polarised signals. As we stressed in the previous Section, the relevant information for the CMB polarised signal can be conveniently read in a non-local combination of Q and U , represented by the E and B modes (see Zaldarriaga, Seljak 1997 and Kamionkowski, Kosowsky, Stebbins 1997). We simulate sky maps for Q and U and perform separation for each of them separately. Let these multi-frequency maps be represented by \mathbf{x}^Q and \mathbf{x}^U respectively, where \mathbf{x} is made of two indexes, labeling frequencies on rows and pixel on columns. If the unknown components to be recovered from the input data scale rigidly in frequency, which means that each of them can be represented by a product of two functions depending on frequency and space separately, we can define a spatial pattern for them, which we indicate with \mathbf{s}^Q and \mathbf{s}^U . Then we can express the inputs $\mathbf{x}^{Q,U}$ as

$$\mathbf{x}^{Q,U} = \mathbf{A}^{Q,U} \mathbf{B} \mathbf{s}^{Q,U} + \mathbf{n}^{Q,U}, \quad (2)$$

where the matrix $\mathbf{A}^{Q,U}$ scales the spatial patterns of the unknown components to the input frequencies, thus having a number of rows equal to the number of input frequencies; the instrumental noise \mathbf{n} has same dimensions as \mathbf{x} . The matrix \mathbf{B} represents the beam smoothing operation: we recall that at the present level of architecture, an ICA based component separation requires to deal to maps having equal beams at all frequencies. Separation is achieved in the real space, by estimating two separation matrices, \mathbf{W}^Q and \mathbf{W}^U , having a number of rows corresponding to the number of independent components and a number of columns equal to the frequency channels, which produce a copy of the independent components present in the input data:

$$\mathbf{y}^Q = \mathbf{W}^Q \mathbf{x}^Q, \quad \mathbf{y}^U = \mathbf{W}^U \mathbf{x}^U. \quad (3)$$

All the details on the way the separation matrix for FASTICA is estimated are given in Maino et al. (2002). \mathbf{y}^Q and \mathbf{y}^U can be combined together to get the E and B modes for the independent components present in the input data (see Zaldarriaga, Seljak 1997 and Kamionkowski, Kosowsky, Stebbins 1997); note that failures in separation for even one of Q and U affect in general both E and B , since each of them receive contributions from both Q and U . It is possible, even in the noisy case, to check the quality of the resulting separation by looking at the product $\mathbf{W}\mathbf{A}$, which should be the identity in the best case: this means that the frequency scalings of the recovered components can be estimated: as in Maino et al. (2002), by indicating as $x_{\nu,j}^{Q,U}$ the j -th component in the data \mathbf{x} at frequency ν , it can be easily seen that the frequency scalings are simply the ratios of the column elements of the matrices \mathbf{W}^{-1} :

$$\frac{x_{\nu,j}^{Q,U}}{x_{\nu',j}^{Q,U}} = \frac{(\mathbf{W}^{Q,U})_{\nu,j}^{-1}}{(\mathbf{W}^{Q,U})_{\nu',j}^{-1}}. \quad (4)$$

However, it is important to note that even if separation goes virtually perfect, which means that $\mathbf{W}\mathbf{A}$ is exactly the identity, equations (2,3) imply that noise is transmitted on the FASTICA outputs, even if it can be estimated and, to some extent, removed as we describe below.

3.2 Instrumental noise

We described how to deal with instrumental noise in a FASTICA based separation approach in Maino et al. (2002), for total intensity maps. A step before the separation process, the noise correlation matrix, which for a Gaussian, uniformly distributed noise is null except for the noise variances at each frequency on the diagonal, is subtracted from the total signal correlation matrix; the “denoised” signal correlation matrix enters then as input in the algorithm performing separation. The same is done also here, for Q and U separately. Moreover, in Maino et al. (2002) we described how to estimate the noise of the FASTICA outputs. In a similar way, let us indicate the input noise patterns as $\mathbf{n}^{Q,U}$. Then from (2,3) it can be easily seen that the noise on FASTICA outputs is given by

$$\mathbf{n}_y^{Q,U} = \mathbf{W}^{Q,U} \mathbf{n}^{Q,U}, \quad (5)$$

which means, if the noises on different channels are uncorrelated, and indicating as $\sigma_{\nu,j}$ the input noise *rms* at frequency ν_j , that the noise *rms* on the i -th FASTICA output is

$$\sigma_{y_i}^{Q,U} = \sqrt{\sum_j |W_{ij}^{Q,U}|^2 \sigma_{\nu,j}^{Q,U}^2}. \quad (6)$$

On whole sky signals, the contamination to the angular power spectrum coming from a uniformly distributed, Gaussian noise characterized by σ is $C_{\ell} = 4\pi\sigma^2/N$, where N is the pixel number on the sphere. The noise contamination to C_{ℓ} s on Q and U can therefore be estimated easily on FASTICA outputs once $\sigma_{\nu,j}^{Q,U}$ in (6) are known. Gaussianity and uniformity makes also very easy to calculate the noise level on E and B modes, since they contribute at the same level; thus we can estimate the noise contamination in the E and B channels as

$$C_{\ell y_i}^E = C_{\ell y_i}^B = \frac{C_{\ell y_i}^Q + C_{\ell y_i}^U}{4} = \frac{\pi(|\sigma_{y_i}^Q|^2 + |\sigma_{y_i}^U|^2)}{N}, \quad (7)$$

where the factor 4 is due to the normalization according to the HEALPix scheme, featuring conventions as Kamionkowski, Kosowsky, Stebbins (1997), whereas the other common version (Zaldarriaga, Seljak 1997) would yield a factor 2. The quantities defined in (7) represent the average noise power, which can be simply subtracted from the output power spectra by virtue of the uncorrelation between noise and signal; the noise contamination is then represented by the power of noise fluctuations around the mean (7):

$$\Delta C_{\ell y_i}^E = \Delta C_{\ell y_i}^B = \sqrt{\frac{2}{2\ell+1}} \left[\frac{\pi(|\sigma_{y_i}^Q|^2 + |\sigma_{y_i}^U|^2)}{N} \right]. \quad (8)$$

Note that the noise estimation is greatly simplified by our assumptions: with a non-Gaussian and/or non-uniform noise, as well as a non-zero Q/U noise correlation etc. could lead for instance to non-flat noise spectra for C_{ℓ} s, as well as non-equal

noises in E and B modes. However, if a good model of these effects is available, a Montecarlo pipeline is still conceivable by calculating many realisations of noise to find the average contamination to E and B modes to be subtracted from outputs instead of the simple forms (7,8).

4 PERFORMANCE STUDY

In this Section we study our approach on simulated skies; we want to assess (*i*) the ultimate capability of FASTICA to clean the CMB maps from synchrotron, i.e. by switching off the noise, (*ii*) how the results degrade as noise is considered.

4.1 Noiseless separation

We adopt a reference angular resolution of 3.5 arcminutes, corresponding to $n_{side} = 1024$ in an HEALPix environment (Górski et al. 1999); this is enough to test the performance of the CMB polarisation reconstruction, in particular for the undamped sub-degree acoustic oscillations, extending up to $\ell \simeq 2000$ in Fig. (2). In all the cases we show, the computing time to achieve separation was of the order of a few minutes on a Pentium IV 1.8 GHz processor with 512 Mb RAM memory. We perform separation by considering the CMB model defined in (1) and as foreground emission both the S_G and S_B models by Giardino et al. (2002) and Baccigalupi et al. (2001), respectively. As we already mentioned, FASTICA performance turns out to be stable with respect to the relaxation of rigid frequency scalings, at least for what concerns the level of spectral index variation exposed in Fig. 3. In order to expose this point in detail, we compare the quality of the CMB reconstruction assuming either constant and varying synchrotron spectral index, indicated with β in the following.

In Fig. 4 we plot the original (dotted) and reconstructed (solid) $C_\ell^{E,B}$'s for CMB, for the S_B foreground emission model. In the left panels, we used a uniform spectral index for synchrotron, while in the right ones it is let to vary. Upper and lower panels represent the 70, 100 GHz and 30, 44 GHz frequency combinations, respectively, used as inputs for the FASTICA algorithm. The same analysis has been performed also for the S_G model for the synchrotron emission, again with constant or space varying synchrotron spectral index, and for the same frequency channels used in the S_B case: the results are plotted in Fig. 5. The cases plotted in the left panels of Figs. 4 and 5 represent the best result achievable, since no noise is considered and the synchrotron spectral index is not varying. As it can be seen, the CMB signal is well reconstructed on all relevant scales, extending up to the pixel size. The same is true for the synchrotron emission, which we do not show. Percent precision in frequency scaling recovery for CMB and synchrotron is reported in Table 1; as we stressed in the previous Section, the precision on frequency scaling recovery corresponds to the precision of the estimation of the elements in the inverse of the matrices \mathbf{W}^Q and \mathbf{W}^U : Table 1 shows how such precision, for both CMB and synchrotron, reaches the percent level or better. Let us focus on the reconstructed B modes; as we already mentioned, CMB is a peculiar component in the sense that it predicts E modes largely dominant over B ones, while for foregrounds E and B modes are expected to have amplitude. Remarkably, FASTICA is able to recover the CMB B modes on all the relevant angular scales, even if they are largely subdominant with respect to the foreground emission. This remarkable result is due to the difference of the underlying statistics describing CMB and foreground emission, which is an expected feature due to their markedly different physical origin. Note also that in the noiseless case with constant synchrotron spectral index, the CMB power spectrum is reconstructed at the same good level both for the 100, 70 GHz and for 30, 44 GHz channel combinations, although in this frequency range the synchrotron emission changes amplitude by a factor of about 10. Indeed, by comparing top and bottom left panels of Figs. 4 and 5, one can note that there is only a minimum difference in the B spectra at 44 GHz and at 100 GHz, arising at high ℓ , while the E spectra exhibit no appreciable difference at all.

Right panels of Figs. 4 and 5 reports the corresponding results for the varying spectral index case. A rigorous component separation would be virtually impossible in this case, since one of the fundamental assumption of any algorithm proposed so far is badly violated; however FASTICA is able to approach convergence by estimating a sort of “mean” foreground emission, scaling roughly with the mean value of the spectral index mapped in Fig. 3. The results of this remarkable stability depend on the amount of residual synchrotron contamination on the CMB reconstructed maps; this residual will be proportional to the difference between the “true” synchrotron emission pattern and the “mean” one, so the deviations of the spectral index β with respect to its mean value will affect CMB reconstruction mainly at the lowest frequencies, where the synchrotron contamination to the CMB signal is more relevant. As it is evident in the right, top panels of Figs. 4 and 5, showing the 70, 100 GHz combinations, CMB E modes are still well reconstructed on all scales; even CMB B modes are reconstructed at least up to their maximum around $\ell \simeq 100$; synchrotron contaminations due to the non-perfect separation appears on the small angular scales tail, and is more relevant in the S_G case it predicts a stronger foreground emission on those scales. As expected, the separation quality degrades substantially in the worst case, i.e. non-uniform β , 30 and 44 GHz combination, represented in the right, bottom panels of Figs. 4, 5. Contamination appears in the CMB E modes, on scales where synchrotron is relevant, i.e. at $\ell \lesssim 200$, while B modes are severely affected on all scales. The worst, as expected, is found in the S_G model in the combination 30, 44 GHz; reconstructed E modes have wrong amplitude and shape at low multipoles, while B modes are almost

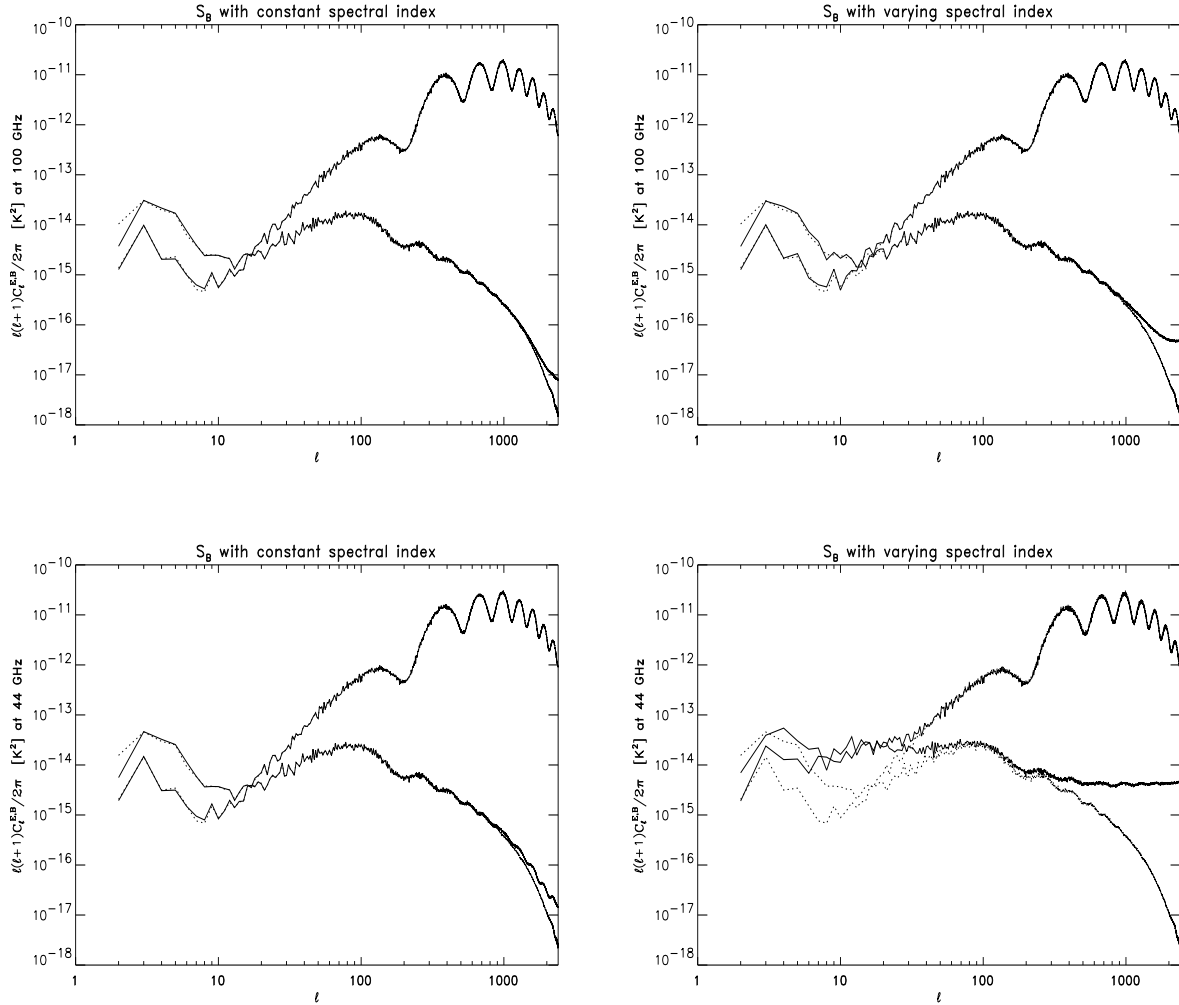


Figure 4. Original (dotted) and reconstructed (solid) power spectra for E and B CMB modes in the S_B model, in the noiseless case. Left panels: constant spectral index. Right panels: space varying spectral index. Upper panels are from inputs at 70 and 100 GHz channels, while bottom panels corresponds to inputs at 30 and 44 GHz.

lost. These results are also reflected in Table 1, where we report the percentage precision in recovering frequency scaling for all the cases considered here. As we already noted, for synchrotron constant spectral index the precision is at percent level or better in all cases. For varying spectral index the precision we quote is respect to a mean frequency scaling defined as $\langle (\nu_1/\nu_2)^\beta \rangle$ where β varies across the sky as in Fig. 3 and the average is taken over all the sky. In this case the frequency scaling reconstruction for CMB is failing in the 30, 44 GHz case, where the synchrotron, in addition to be not rigidly scaling in frequency, has higher amplitude; the level of degradation is higher in the S_G case since it yields a higher contamination with respect to the S_B model.

4.2 The effect of noise

Here we study the effect of the noise on the separation performance. For our purposes here, a map resolution of about 7 arcminutes, corresponding to $n_{side} = 512$ in an HEALPix scheme (Górski et al. 1999), is enough: at this resolution the separation runs take a few seconds on the whole sky; moreover we consider the combination 70, 100 GHz only, and a space varying synchrotron spectral index. We parametrize the noise with the signal to noise ratio (S/N) between the CMB and the noise rms . As we already stressed, noise is either subtracted during the separation process, and on the reconstructed C_ℓ , according to the estimate in equation (7); results are affected by the residual noise fluctuations, with power given by (8).

By switching on the noise, the reconstruction of CMB B modes is affected first. In Fig. 6 we plot the reconstructed and

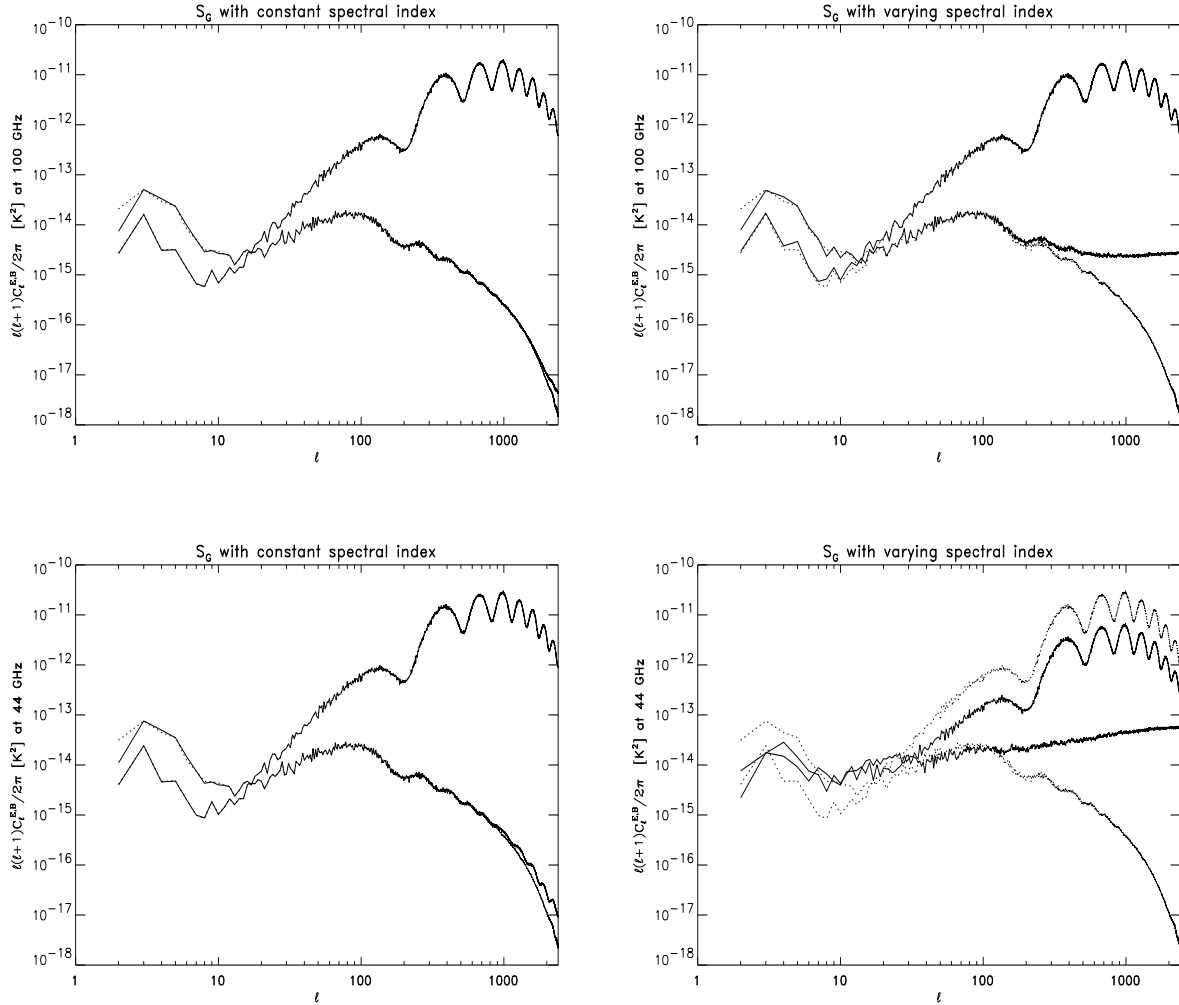


Figure 5. Original (dotted) and reconstructed (solid) power spectra for E and B CMB modes in the S_G model, in the noiseless case. Left panels: constant spectral index. Right panels: space varying spectral index. Upper panels are from inputs at 70 and 100 GHz channels, while bottom panels corresponds to inputs at 30 and 44 GHz.

original CMB E and B modes, for S_G (left) and S_B (right) foreground emission, in the case $S/N = 2$. With this level of noise, separation is still successful: E modes are substantially unaffected, while B modes are well reconstructed up to the characteristic peak at $\ell \simeq 100$, while the noise residual becomes important on larger multipoles, where the original signal is dumped out. This features are also reflected by the numbers in Table 2, where we report the precision of frequency scaling recovery, for CMB, in the noisy case: the precision remains at the percent level both for Q and U .

By further decreasing S/N , B modes get lost, while still the algorithm is successful in recovering the E power. This holds until the noise level gets so high that the separation matrix is seriously affected and the algorithm fails; on the power spectra, this failure manifests in a contamination of the E modes by synchrotron, on the low multipole tail, say $\ell \lesssim 100$, where synchrotron dominates with respect to CMB, both in the S_G and S_B cases, see Fig. 2. In Fig. 7 we report the result of separation when $S/N = 0.2$ in the S_G case (left) and $S/N = 0.5$ in the S_B case (right). Top panels report E modes: the spurious power on low multipoles, deriving from synchrotron contamination as a result of the non-perfect separation, is well evident on both cases. For the S_G case, where noise is higher, we average over 8 multipoles in order to avoid oscillations going negative on the recovered spectrum. B modes are lost on all scales, as bottom panels show. Correspondingly, Table 2 shows the degradation of the separation matrix with respect to the previous case with $S/N = 2$; note that, due to the high level of foreground contamination on the scales considered, power spectrum recovery is failing even if the separation matrix, as seen as the percentage errors on frequency scaling recovery in Table 2, is only marginally affected. The reason of the difference between the S/N at which separation fails in the S_G and S_B cases is the different overall amplitude of the

Table 1. Percentage errors on frequency scalings reconstruction in the noiseless case.

Synchrotron S_G model	const. β		variable β	
Frequency range (GHz)	30, 44	70, 100	30, 44	70, 100
Q synch.	1.48×10^{-2}	0.11	21.73	7.55
U synch.	5.71×10^{-3}	4.56×10^{-2}	21.73	7.55
Q CMB	0.31	2.69×10^{-2}	207.36	1.18
U CMB	0.69	5.83×10^{-2}	222.12	1.21
Synchrotron S_B model	const. β		variable β	
Frequency range (GHz)	30, 44	70, 100	30, 44	70, 100
Q synch.	0.18	1.46	19.19	1.04
U synch.	0.137	1.10	19.73	1.04
Q CMB	1.01	8.79×10^{-2}	6.15	9.62×10^{-2}
U CMB	0.1448	1.24×10^{-2}	9.028	0.107

Table 2. Percentage errors on CMB frequency scalings reconstruction in the noisy case by considering 70, 100 GHz input channels.

Synchrotron S_G model	$S/N = 2$	$S/N = 0.2$
Q CMB	1.04	13
U CMB	0.66	0.89
Synchrotron S_B model	$S/N = 2$	$S/N = 0.5$
Q CMB	0.31	4.26
U CMB	0.34	0.35

synchrotron contamination in the two cases. Since the S_G model has a higher amplitude, FASTICA is able to catch statistics more efficiently than for S_B , thus being able to work up to a higher level of noise.

Ultimately, when the noise level is so high that the all input maps get dominated by the noise itself, the algorithm ultimately fails in converging to any component.

We conclude by stressing that the noise levels quoted here are not the maximum level of noise which the algorithm supports. The performance of the separation depends on the noise level as well as on the number of the channels considered; adding more channels, while keeping constant the number of components to recover, generally improves the statistical sample with which FASTICA deals and so the quality of the reconstruction as well as the amount of noise supported. In the next Section we show an applied example where a satisfactory separation can be obtained with higher noise by considering a combination of three frequency channels.

5 APPLICATION TO PLANCK-LFI

In this Section, we apply FASTICA to extract the polarised CMB component from the sky as seen by an instrument performing as PLANCK-LFI (see <http://astro.estec.esa.nl/SA-general/Projects/Planck> for details). Such instrument is composed by four frequency channels, 30, 44, 70 and 100 GHz, having full width half maximum (FWHM) corresponding to 33, 23, 14 and 10 arcminutes, respectively. We assess the instrumental capability to recover E , B and TE modes, separately. The noise level is taken according to the nominal performances, increasing the noise rms given for total intensity by a factor $\sqrt{2}$ corresponding to the polarisation measurements (note also that due to the HEALPix convention to normalize Q and U following the prescription by Kamionkowski, Kosowsky and Stebbins 1997, a further $\sqrt{2}$ has to be taken into account when generating Q and U maps out of a given power in E and B). We neglect all instrument systematics in this work. We also provide a comparison with the expectation of the MAP satellite, for polarisation measurements and in presence of foregrounds.

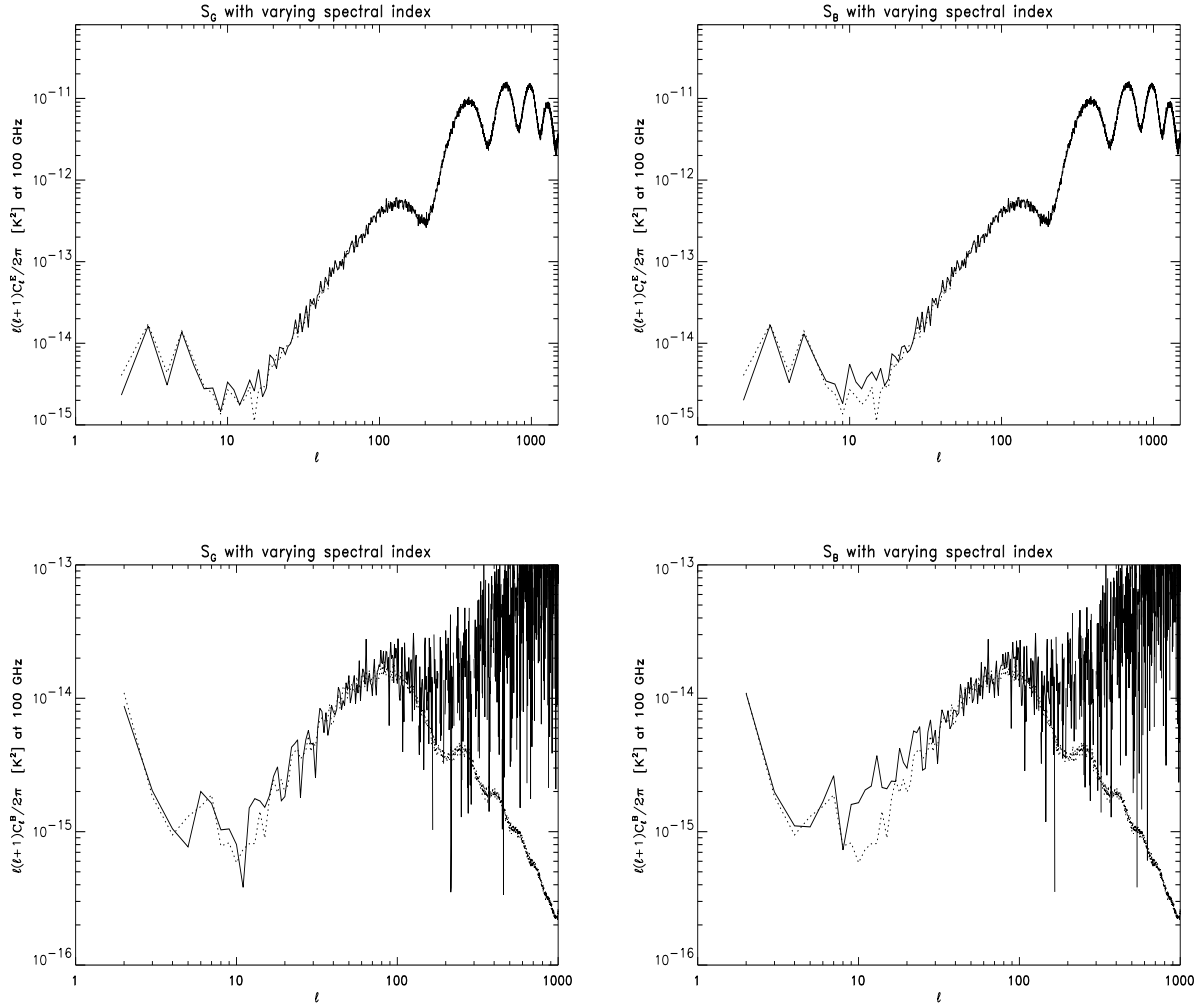


Figure 6. Original (dotted) and reconstructed (solid) power spectra for E (top) and B (bottom) CMB modes for the S_G (left) and S_B (right) cases, assuming $S/N=2$ and considering 70 and 100 GHz; the synchrotron spectral index is space varying.

The LFI and MAP instrumental features, with noise rms in antenna temperature calculated for a pixel size of about 3.52 arcminutes corresponding to $nside = 1024$ in the HEALPix scheme, are summarized in Table 3. By looking at the numbers, it can be immediately realized that the level of noise is sensibly higher than the one considered in the previous Section, so that the same method would not work in this case and an improved analysis, involving more channels as described below, is necessary.

5.1 E modes

Due to the high level of noise, we found convenient to include in the analysis the lower frequency channels together with 70 and 100 GHz. Since the FASTICA algorithm is unable to deal with channels having different FWHM, as in Maino et al. (2002), we had to degrade the maps, containing both signal and noise, to the worst resolution in the channels considered. However, a satisfactory recovery of the CMB E modes, extending on all scales up to the instrument best resolution, is still possible by making use of the different angular scale properties of both synchrotron and CMB. Indeed, as it can be seen in Fig. 2, the Galaxy is likely to be a substantial contaminant on low multipoles, say $\ell \lesssim 200$; by including the lower frequency channels we still perform separation where the synchrotron contamination is relevant, but we exploit the major advantage to add the lower frequency channels to the database input to FASTICA. We expose now the results of this strategy, leaving the recovery of the CMB signal at larger multipoles, corresponding to a degree or less, to another approach which is exposed below.

For the present application, we found convenient to use a combination of three PLANCK channels, 44, 70, 100 GHz for

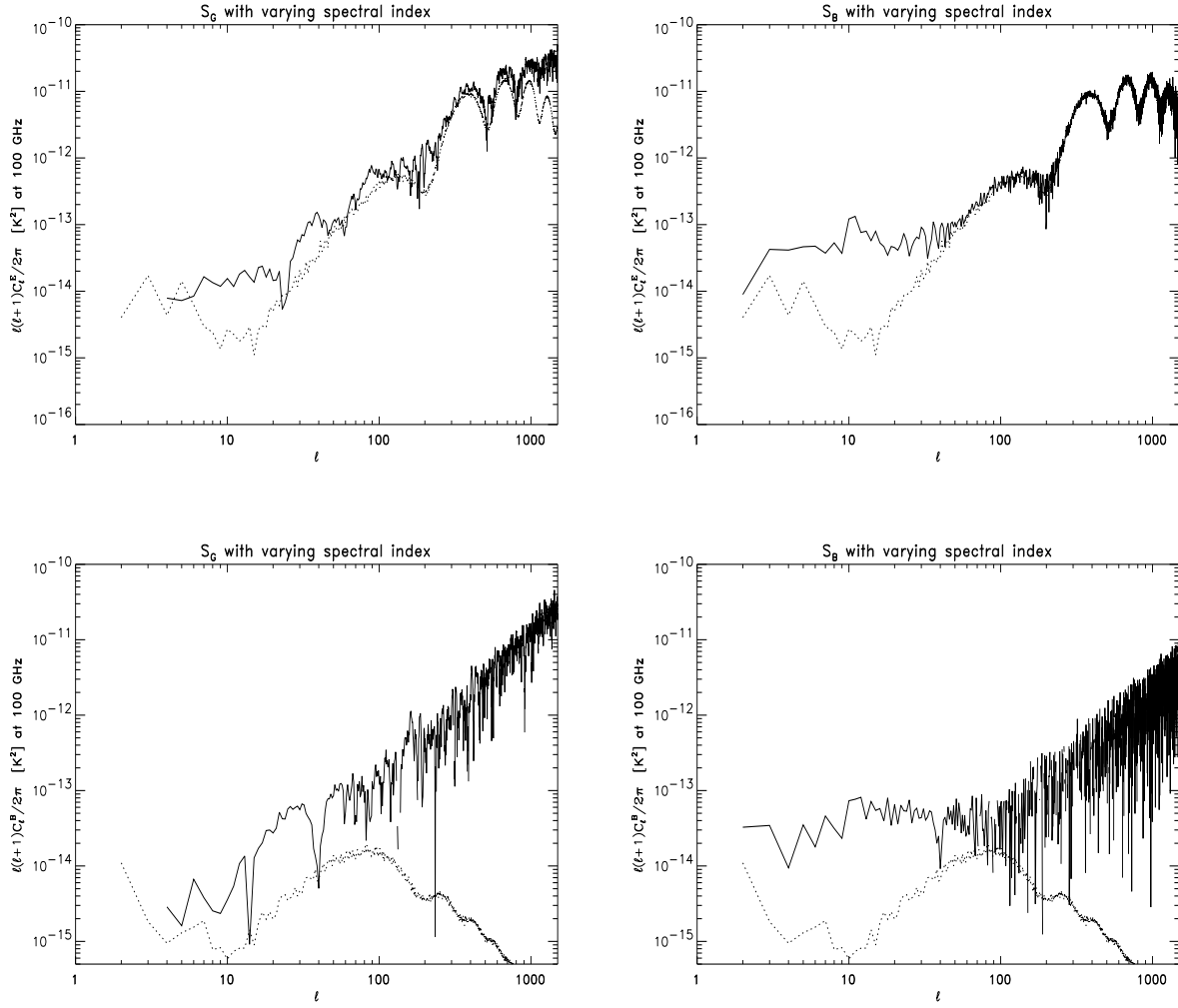


Figure 7. Original (dotted) and reconstructed (solid) power spectra for E (top) and B (bottom) CMB modes for the S_G (left, assuming $S/N = 0.2$, averaged over 8 multipole intervals) and S_B (right, assuming $S/N = 0.5$) cases, considering 70 and 100 GHz; the synchrotron spectral index is space varying.

Table 3. PLANCK-LFI and MAP nominal performances; MAP noise correspond to a four year observation period.

Frequency (GHz, LFI)	30	44	70	100
FWHM (arcmin.)	33	23	14	10
noise <i>rms</i> for 3.52' pixels (μK)	80	81	69	52
Frequency (GHz, MAP)	22	30	40	60
FWHM (arcmin.)	56	41	32	21
noise <i>rms</i> for 3.52' pixels (μK)	250	247	243	230
			206	

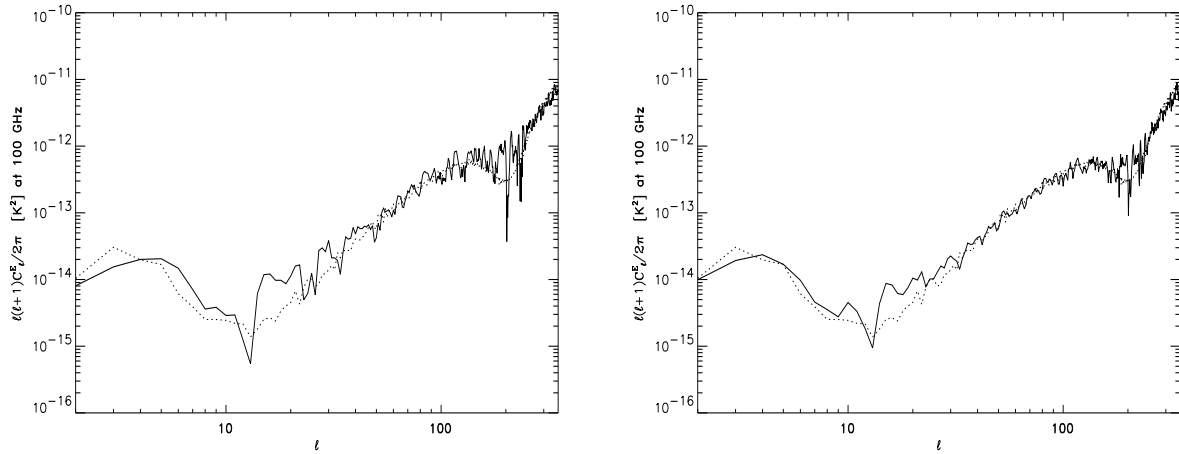


Figure 8. Original (dotted) and reconstructed (solid) CMB C_ℓ^E obtained by applying the FASTICA algorithm to the combinations 44, 70, 100 GHz for the S_G synchrotron case (left) and 30, 70, 100 GHz for the S_B model (right).

the S_G and 30, 70, 100 GHz for the S_B models, respectively. The reason of the difference is that the S_B contamination is weaker, and the 30 GHz channel is necessary for FASTICA to catch synchrotron with enough accuracy. Including a fourth channel does not imply relevant improvements. The maps, including signals properly smoothed and noise according to the Table 3, were simulated at 3.52' resolution, corresponding to $n_{side} = 1024$; higher frequency maps were then smoothed to the FWHM of the lowest frequency channel and then re-gridded to $n_{side} = 128$, corresponding to a pixel size of about 28' and to a maximum multipole $\ell \simeq 400$. In all the results shown, the spectral index for synchrotron has been considered variable. Fig. 8 shows the resulting CMB E mode power after separation, for the S_G (left) and S_B (right) synchrotron models. An average every 4 (left) and 3 (right) coefficients was applied to eliminate fluctuations going negative on the lowest signal part at $\ell \simeq 10$. The agreement between the original spectrum and the reconstructed one is good on all the scales probed at the present resolution, up to $\ell \simeq 400$. The reionization bump is clearly visible as well as the first polarisation acoustic oscillation at $\ell \simeq 100$. Moreover, no evident difference can be noted about the quality of the reconstruction between the two models of foreground adopted.

Unfortunately, the same strategy applied to MAP does not produce any result. The reason is the high level of noise, which is likely to hide not only the CMB but also most of the Galactic polarised signal. A blind algorithm like FASTICA is not able to work in these conditions since it needs to catch at least one non-Gaussian signal in the database to work (see Maino et al. 2002). In heavy noisy situations like the case of MAP, the code fails to converge to any component simply because the statistics of the database is dominated by the Gaussianity of the instrumental noise.

Let us turn now to the degree and sub-degree angular scales, $\ell \gtrsim 200$. As we already stressed, the Galaxy is expected to yield an approximately equal power on E and B modes, see Fig. 2; on the other hand, CMB E and B modes are dramatically different on sub-degree angular scales: summarizing, on $\ell \gtrsim 200$, we expect to have

$$C_\ell^{E Gal} \simeq C_\ell^{B Gal}, \quad C_\ell^{E CMB} \gg C_\ell^{B CMB}. \quad (9)$$

Therefore, on $\ell \gtrsim 200$ where the CMB contamination from synchrotron is expected to be irrelevant, the power spectrum of the CMB E modes can be estimated by simply subtracting, together with the noise, the B power as

$$C_\ell^{E CMB} \simeq C_\ell^{E CMB+Gal} - C_\ell^{B CMB+Gal} - C_\ell^{E noise}, \quad (10)$$

where the total map CMB+Gal is used without any separation procedure. In other words, there is no need to perform separation to get the CMB E modes at high multipoles, because they are simply obtained by subtracting the B modes of the sky maps, since the latter are dominated by synchrotron which has almost equal E and B modes. Fig. 9 shows the results of this technique applied to the PLANCK-LFI 100 GHz channel, for both the S_G and S_B synchrotron models. Residual fluctuations are higher in the S_G case since the synchrotron contamination is stronger. In both cases, CMB E modes are successfully recovered in the whole interval $100 \lesssim \ell \lesssim 1000$. It has also to be noted that the same subtraction technique would not help on the lower multipoles considered before, since in that case the foreground contamination is so strong that the tiny fluctuations making Galactic E and B modes different are likely to hide the CMB signal anyway.

The results of the same technique applied to MAP are again much worse due to the higher instrumental noise, yielding a major contaminant from the last term in (10). However, some result can be achieved by applying the method expressed

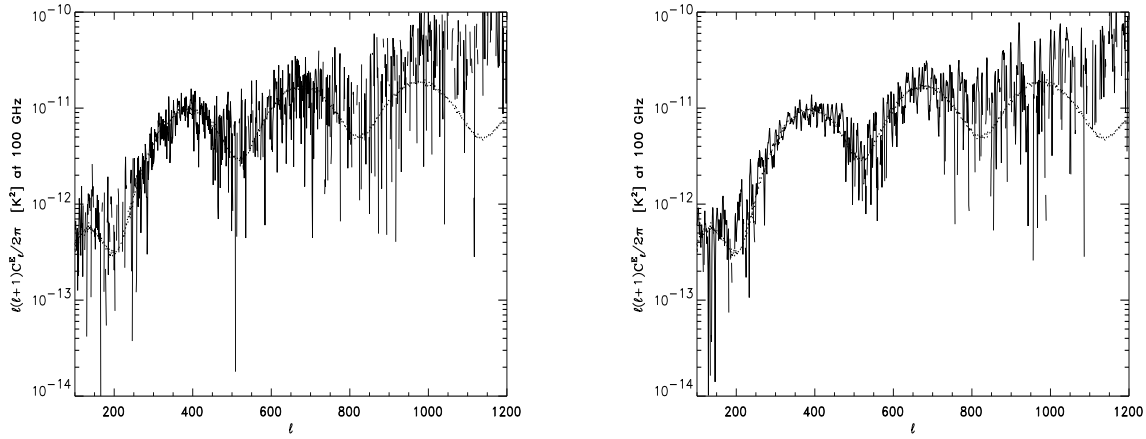


Figure 9. Original (dotted) and reconstructed (solid) CMB C_ℓ^E obtained by subtracting the expected level of noise as well as the synchrotron contaminations S_G (left) and S_B (right) assumed almost coincident as the power of the B map. The assumed instrumental features are those of the PLANCK-LFI channel at 100 GHz.

by (10) on the three highest frequency MAP channels, at 40, 60 and 90 GHz, and than averaging over the three $C_\ell^{E\,CMB}$ obtained; before the averaging process the maps have been brought to the same resolution by dividing the spectra for the beam window function at the corresponding frequency. This procedure allows to reach a marginal detection of the second acoustic oscillation of E modes, located at multipoles between 300 and 400, which is indeed the highest part of the signal in the acoustic oscillation region, as it can be seen by looking at Fig. 2 and comparing to the ℓ^2 behavior of the noise. The result is shown in Fig. 10, for the S_G (left) and S_B (right) synchrotron models. Again, the dotted line is the original spectrum, while the solid one is what it is obtained by averaging over 60 multipoles, which is necessary because of the high level of noise fluctuations which are still dominant after averaging over the three channels considered: the amplitude of the noise fluctuations, corresponding to the quantities (8) averaged over the three channels considered, are plotted in the small boxes showing the original (dotted) spectrum and the noise fluctuation power (solid). Relatively to the CMB signal, the noise contamination has actually a minimum nearby the second CMB acoustic oscillation where we have detection: on smaller multipoles the CMB signal drops approaching the behavior on large angular scales, while on larger multipoles the noise explodes because of the division by the window function.

Our results here can be summarized as follows: by exploiting the existing component separation algorithms, even in presence of severe polarised Galactic contamination, by assuming the PLANCK-LFI nominal performances it is possible to clean the maps from foreground emission and restore the performance that the instrument would have *in absence* of foregrounds: the detection of CMB E modes covers all multipoles up to the instrumental angular resolution, up to $\ell \simeq 1000$. By assuming the MAP performances, yielding a substantially higher noise contamination, a marginal detection of the highest part of the second CMB acoustic oscillation is possible, at multipoles $300 \lesssim \ell \lesssim 400$.

In the next Section we show the results of the FASTICA technique in terms of the recovery of the CMB B modes.

5.2 B modes

As we already stressed in the Introduction, cosmological B modes for CMB polarisation are not excited by primeval density perturbations; in absence of primordial vector perturbations, cosmological sources of B modes in CMB anisotropies are gravitational waves, appearing on all multipoles corresponding to super-horizon cosmological scales at decoupling, say $\ell \lesssim 200$; an independent mechanism generating B modes is represented by the reionisation process, expected to occur at relatively low redshifts compared to the decoupling time: it manifests as a bump appearing at very low multipoles, say $\ell \lesssim 10$. Consequently, B mode detection would have great importance since it could reveal insight on the nature of the mechanisms generating perturbations in the very early universe, as well as on the ionisation history of the universe. Unfortunately, while a reionisation process is somewhat expected (and actually our optical depth to reionisation is consistent with recent estimates by Becker et al. 2001) there are presently no strong evidences non-zero amplitude of cosmological gravitational waves (Baccigalupi et al. 2002a), even if constraints are not too tight at due to the accuracy of present CMB data. We show here that FASTICA allows the recovery of the B low multipoles, where the signal is high because of the reionisation bump, as well as a marginal evidence for the B signal associated to gravitational waves, if the latter have at least the amplitude we choose, a fraction 30%

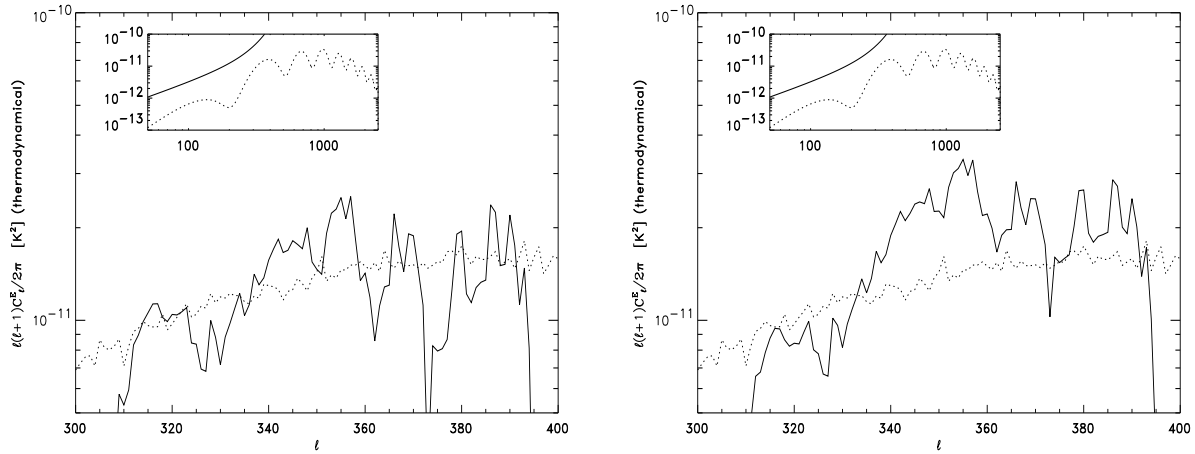


Figure 10. Original (dotted) and reconstructed (solid) CMB C_ℓ^E obtained by applying the same technique as in Fig. 9 on the three MAP channels at 40, 60, 90 GHz and averaging. A further average over 60 multipoles was applied; boxes show the noise fluctuation power (solid) represented by (8) averaged on the three MAP channels.

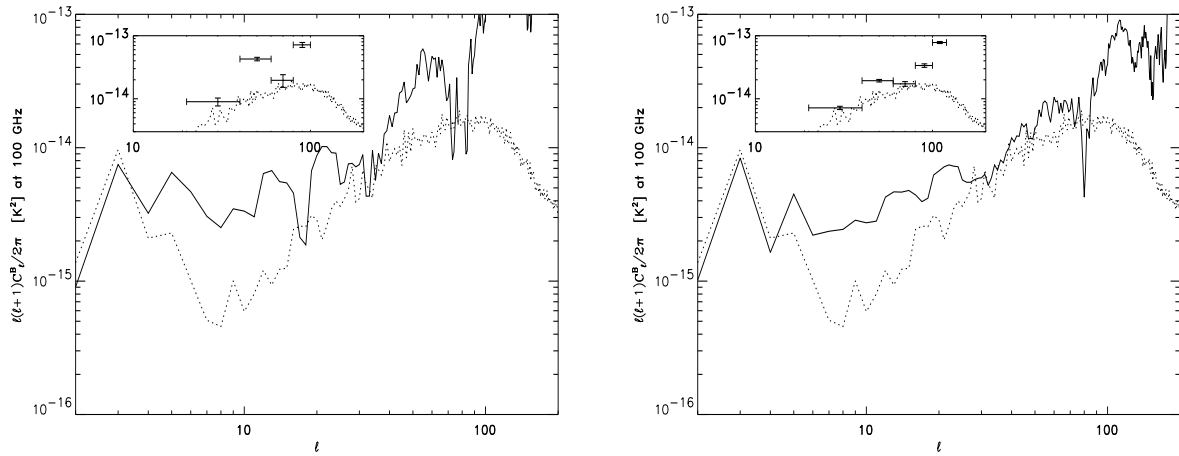


Figure 11. Original (dotted) and reconstructed (solid) CMB C_ℓ^B obtained by applying the FASTICA algorithm to the PLANCK-LFI combinations 44, 70, 100 GHz for the S_G synchrotron case (left) and 30, 70, 100 GHz for the S_B model (right); boxes show data in the range $30 \leq \ell \leq 120$ by considering combinations of 20 multipoles and error bars given by (8).

of scalar perturbations. Lower gravitational waves amplitude is likely to be beyond the capabilities of the present technique when applied to PLANCK-LFI. No result is achievable by assuming the MAP performance.

In Fig. 11 we show the B amplitude after FASTICA separation described in the previous section is shown for the S_G (left) and S_B (right) synchrotron models. An average every 13 multipoles has been applied to both cases in order to avoid fluctuations going negative. The reconstructed signal approaches the original one at very low multipoles, say $\ell \lesssim 5$. At higher multipoles, where the B signal is generated by gravitational waves, the overall amplitude appears to be recovered, even if with major contaminations especially in the region where the signal is low, i.e. right between the reionisation bump and the raise toward the peak at $\ell \simeq 100$; needless to say, such contaminations are due to a residual foreground emission in the CMB maps due to a non-perfect separation process. It is useful to study in more detail the quality of the B mode recovery at multipoles $\ell \lesssim 100$. In the boxes of Fig. 11 we report the data we get by considering combinations of 20 multipoles and averaging the noise as given by (8) in the range between $30 \leq \ell \leq 120$: even if the contamination is substantial, especially for $\ell \geq 100$ and for the S_G case, the data partially track the characteristic rise of the spectrum due to cosmological gravitational waves.

Concluding, we can claim a substantial recovery of the B lowest multipole signal if the latter is boosted by a reionisation process as we assume in this work; moreover, our results indicate that the B modes from cosmological gravitational waves can be detected if the tensor to scalar perturbation ratio is at least 30%.

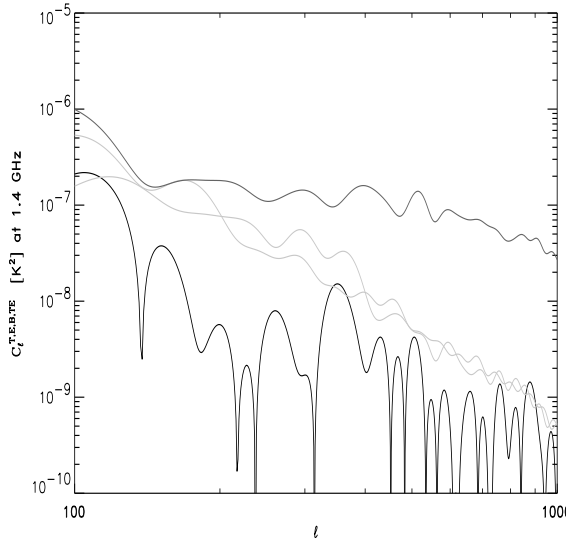


Figure 12. T (solid), E , B (light) and TE (heavy solid) modes in the fan region at medium Galactic latitudes (Uyaniker et al. 1999).

5.3 TE modes

As we already stressed, a strong correlation exists between total intensity and E polarisation modes; the reason is that the latter are primarily excited by the projected quadrupole of scalar perturbations at last scattering (see Hu et al. 1999 and references therein). In addition, TE modes are the strongest, in terms of signal, with respect to any other polarised CMB component, either because of the strong TE correlation, and of the contribution of the total intensity anisotropies, which are roughly one order of magnitude larger with respect to CMB polarisation. It is therefore interesting to forecast the PLANCK-LFI performance in the measurement of the TE CMB spectrum in presence of foregrounds. We also study the expectations from the observations of the MAP satellite, finding results which are consistent with recent estimates (see Kogut, Hinshaw 2000).

Before showing the results it is useful to give our present guess about the level of TE for synchrotron. On degree and sub-degree angular scales, a measure of the synchrotron TE power spectrum can be achieved in the radio band. In the Parkes data at 1.4 GHz, Uyaniker et al. (1999) were able to isolate a region exhibiting pretty low rotation measures, named “fan region”, which is therefore expected to be less affected by Faraday depolarisation. This and other regions from the existing surveys in the radio band were used to predict the synchrotron power for the S_B scenario (Baccigalupi et al. 2001). We compute the T, E, B, TE spectra on the fan region, and we show them in Fig. 12. Total intensity anisotropies are represented by the upper curve (solid). E and B modes (light) have very similar behavior. TE modes (heavy solid) are the weakest; this result is somewhat contrary to the CMB case, where the TE power is the strongest polarisation component. As it can be easily seen by scaling the TE amplitude in Fig. 12 with typical spectra index for synchrotron, the amplitude is markedly below the expected cosmological TE signal at CMB frequencies. Actually, both the synchrotron models S_G and S_B respect this guess: in Fig. 13 we plot the TE modes for CMB versus S_G and S_B models, at 100 GHz; it is straightforward to check that our models for the synchrotron emission have a TE power which is not far from the one in Fig. 12, when scaled at the appropriate frequency.

From the point of view of CMB observations, this means that, if the synchrotron contamination at microwave frequencies is well represented by its signal in the radio band, at least on degree and sub-degree angular scales the contamination from synchrotron is almost absent due to the change in the magnetic field orientation along the line of sight. On the other hand, on larger scales as it can be seen in Fig. 13, the contamination could be relevant both in the S_G and S_B cases and we perform component separation as described in Section 5.1 for the PLANCK-LFI case. In Fig. 14 we show the recovery of the CMB TE modes, obtained by combining the templates of Q and U maps obtained after FASTICA application as in Section 5.1 with the CMB T template obtained, still with FASTICA based component separation strategy, in Maino et al. (2002). Oscillations due to noise residual are visible in the recovered C_ℓ^{TE} ; however, as in the case of E , the procedure was successful in substantially removing the contamination which is visible on the relevant multipoles in Fig. 13.

Let us now consider the CMB TE modes recovery on degree and sub-degree angular scales, for PLANCK-LFI and MAP. Since the contamination both in the S_G and S_B cases is almost absent in the acoustic oscillation region of the spectrum, as it is evident again from Fig. 13, we neglect foreground emission. In Fig. 15 we plot the result for PLANCK, and in Fig. 16 the corresponding ones for MAP. The combination of the angular resolution and sensitivity for PLANCK allow the recovery of the

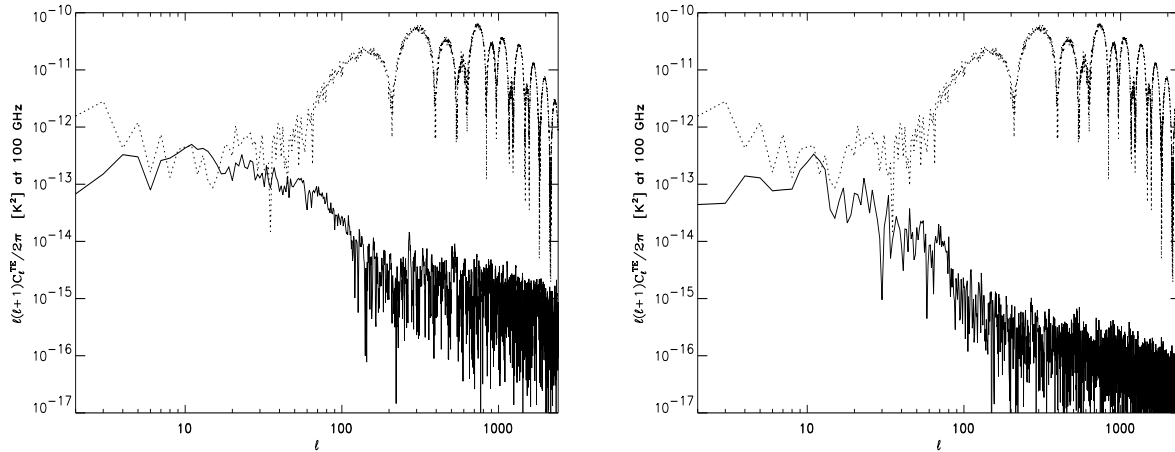


Figure 13. C_ℓ^{TE} of CMB (dotted) versus S_G (solid, left) and S_B (solid, right), at 100 GHz.

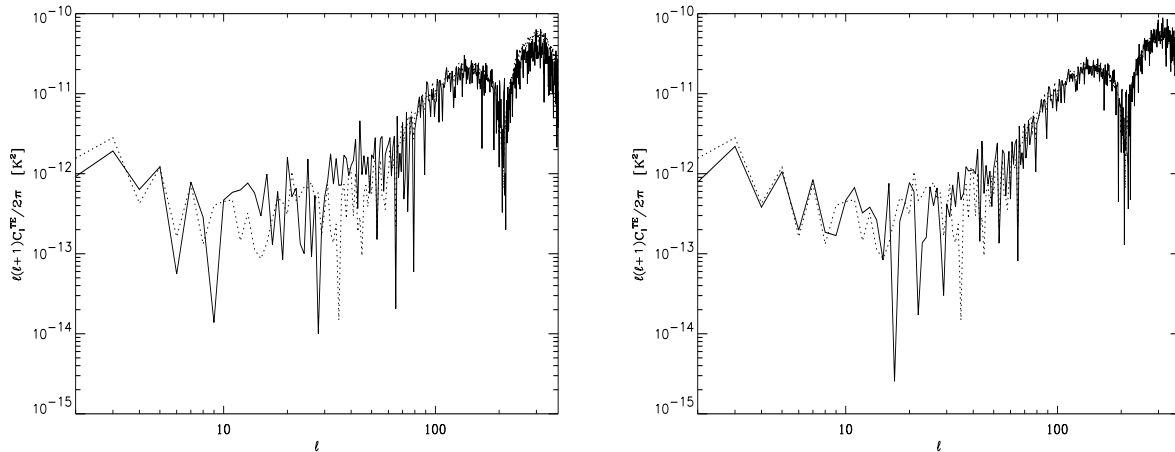


Figure 14. C_ℓ^{TE} of original (dotted) and recovered (solid) CMB emission obtained with FASTICA applied to PLANCK, by considering S_G (left) and S_B (right) foreground model, respectively; results are shown at 100 GHz.

TE spectrum up to arcminutes angular resolution, $\ell \simeq 1200$. Note that this corresponds roughly to the seventh CMB acoustic oscillation. On the other hand, in agreement with earlier estimates (Kogut, Hinshaw 2000), we find that the MAP features are likely to allow a detection up to $\ell \simeq 500$, corresponding to the third CMB TE acoustic oscillation. Note that in the MAP case, since FASTICA is not able to approach convergence due to the level of instrumental noise, we are not able to obtain the recovery of the TE spectrum on larger angular scales as in Fig. 14.

6 CONCLUDING REMARKS

Forthcoming observations of the Cosmic Microwave Background (CMB) anisotropies are expected to measure CMB polarisation. The best performance, for sky coverage, sensitivity and angular resolution is expected to be reached by the PLANCK satellite (see <http://astro.estec.esa.nl/SA-general/Projects/Planck>).

Foreground contamination is mildly known for total intensity measurements, and poorly known for polarisation (see De Zotti 2002 and references therein); it is therefore crucial to develop data analysis tools able to clean the polarised CMB signal from foreground emission by exploiting the minimum number of a priori assumptions. In this work, we implemented the Fast Independent Component Analysis technique (FASTICA, see Amari, Chichocki 1998, Hyvärinen 1999, Maino et al. 2002) for blind component separation to deal with astrophysical polarised radiation.

In our scheme, component separation is performed on the Stokes parameter Q and U maps independently; E and B

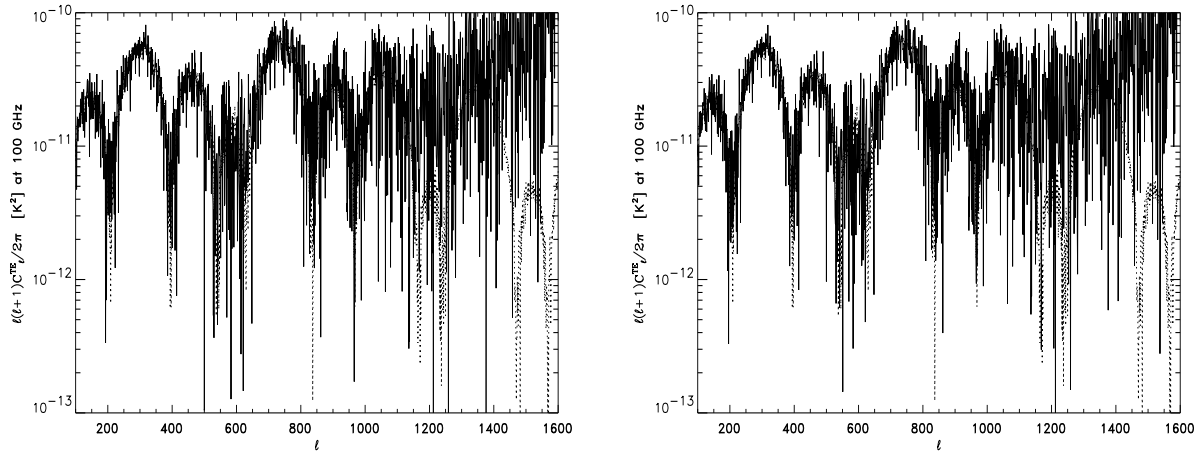


Figure 15. C_ℓ^{TE} of original (dotted) and recovered (solid) CMB emission assuming S_G (left) and S_B (right) as the foreground contaminant, obtained by considering the PLANCK-LFI performances at 100 GHz.

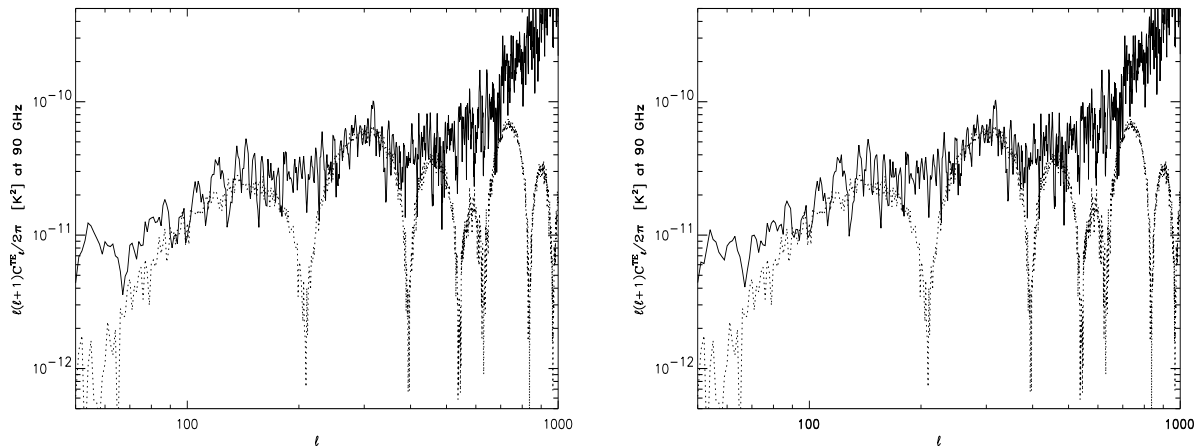


Figure 16. C_ℓ^{TE} of original (dotted) and recovered (solid) CMB emission assuming S_G (left) and S_B (right) as the foreground contaminant, obtained by considering the MAP performances at 90 GHz.

modes, coding CMB physical content in the most suitable way (see Zaldarriaga, Seljak 1997, Kamionkowski, Kosowsky, Stebbins 1997) are then built out of the separation outputs. We described how to estimate the noise on FASTICA outputs, on Q and U as well as on E and B .

We tested this strategy on simulated polarisation microwave all sky maps containing a mixture of CMB and Galactic synchrotron. CMB is modeled in agreement with present measures (De Bernardis et al 2002, Halverson et al. 2002, Lee et al. 2001, Padin et al. 2001), with a component of cosmological gravitational waves at 30% level with respect to density perturbations; we also include a reionisation component, with optical depth at reionisation in agreement with present estimates (Becker et al. 2001). Galactic synchrotron is modeled with the two existing templates by Giardino et al. (2002) and Baccigalupi et al. (2001). These models yield approximately equal power on angular scales above the degree, dominating over the expected CMB power; on sub-degree angular scales, the Giardino et al. (2002) model predict a higher power, but when compared to CMB E mode acoustic oscillation, both models are subdominant. Note that at 100 GHz, the fluctuations at multipoles as high as 1000, corresponding to a few arcmin. angular scales, are likely dominated by compact or flat spectrum radio sources (Baccigalupi et al. 2002b, Mesa et al. 2002); their signal is included in the maps used to estimate the synchrotron power spectrum. We studied in detail the limiting performance in the noiseless case, as well as the degradation induced by a Gaussian, uniformly distributed noise, by considering the frequencies of the Low Frequency Instrument (LFI) aboard the PLANCK satellite. In the noiseless case, the algorithm is able to recover CMB E and B modes on all the relevant scales. In particular, this result is stable against space variation of the synchrotron spectral index according to the existing data.

In this case, FASTICA is able to converge to an average synchrotron component, characterized by a “mean” spectral index across the sky, and to remove it efficiently from the map; the remaining CMB template, also containing residual synchrotron due to its space varying spectral index, is mostly good as far as the frequencies considered are those where the synchrotron contamination is weaker.

By switching on the noise, the recovery of the CMB B modes get degraded first; however, we found that separation, at least for what concerns CMB E modes, is still satisfactory for noise exceeding the CMB but not the foreground emission: the reason is that in these conditions the algorithm is still able to catch and remove the synchrotron component as efficiently as it dominates over the noise.

We perform a worked application of these tools by considering the nominal PLANCK-LFI polarisation performances, in terms of frequencies, angular resolution and noise: our aim is to assess the capability of that instrument to recover CMB E , B , and the total intensity polarisation correlation TE in presence of foregrounds and at the present status of knowledge of blind component separation techniques. To improve the signal statistics, we found convenient to consider at least three frequency channels in the separation procedure, including the ones where the CMB is strongest, 70, 100 GHz, plus one out of the two LFI lower frequency channels, at 30 and 44 GHz. Since the latter have lower resolution we had to degrade the higher frequency maps since the present FASTICA architecture cannot deal with maps having different beam apertures. CMB E and TE modes were accurately recovered for both the synchrotron models considered. B modes are well recovered on very large angular scales if the reionisation causes a bump in their amplitude; on the remaining scales, where their power is mainly due to cosmological gravitational waves, the recovery is only marginal, indicating the assumed amplitude (30% tensor to scalar perturbation ratio) as a B mode detection threshold for the FASTICA capability when applied to the nominal PLANCK-LFI instrumental features.

On the sub-degree angular scales the contamination from synchrotron is almost irrelevant according to both models (Giardino et al. 2002, Baccigalupi et al. 2001). Moreover, it is expected that Galactic E and B modes have approximately the same power (Zaldarriaga 2001), while for CMB the latter are severely damped since they are associated with vector and tensor perturbations, vanishing on sub-horizon scales at decoupling corresponding to a degree or less in the sky (see Hu et al. 1999); this argument holds also if the B mode power is enhanced by weak lensing effects from matter structures along the line of sight (see Hu 2002 and references therein). Therefore, on these scales, we expect the E power spectrum to be a sum of Galactic and CMB contributions, while the B power comes from the Galaxy only: in these conditions, the CMB E power spectrum is recovered by simply subtracting the B power, dominated by the Galaxy and approximately equal to the Galactic E amplitude. We also estimated the TE contamination from synchrotron to be irrelevant for CMB, because of the strength of the CMB TE component due to the intrinsic correlation between scalar and quadrupole modes exciting E polarisation. By applying these considerations on sub-degree angular scales, as well as the results of the FASTICA procedure described above on larger scales, we show how the PLANCK-LFI instrument is capable to recover the CMB E and TE spectra on all scales down to the instrumental resolution, corresponding to a few arcminute scale; in terms of multipoles, E and TE angular power spectrum coefficient are recovered up to 1000 and 1200, respectively.

We also compare the above results with what can be obtained by assuming the nominal performances of the MAP satellite (Wright 1999, see also <http://map.gsfc.nasa.gov/>), operating roughly on the same frequency range as PLANCK-LFI. Unfortunately, the FASTICA technique is not viable because it cannot converge to any component, because of the higher level of instrumental noise compared to PLANCK-LFI. On the other hand, by applying the above considerations on degree and sub-degree angular scales we claim that it could be possible to recover the highest part of the second CMB acoustic oscillation for E modes, corresponding to $300 \lesssim \ell \lesssim 400$, while B modes are lost. For what concerns the TE spectrum, we find that the MAP features should allow to detect the first three acoustic oscillation, in an interval $100 \lesssim \ell \lesssim 500$.

Summarizing, we found that PLANCK-LFI, with nominal performances, is able to recover CMB TE and E modes on all scales extending from the whole sky to a few arcminutes, substantially improving over the expected MAP performances. A marginal detection of B modes is possible if the cosmological tensor amplitude is at least 30% of the scalar one. In particular, we find that on large angular scales, degree and more, foreground contamination is expected to be severe and the known blind component separation techniques are able to efficiently clean the map from such contamination, as it is presently known or predicted.

Still, despite these good results, the main limitation of the present approach is neglecting any instrumental systematics. While it is important to assess the performance of a given data analysis tool in the presence of the nominal instrumental features, as we do here, a crucial test is checking the stability of such tool with respect to relaxation of the assumptions regarding the most common sources of systematic errors, like beam asymmetry, non-uniform and/or non-Gaussian noise distribution etc., as well as the idealized behavior of the signals to recover. In this work we had a good hint about the second aspect, since we showed as FASTICA is stable against relaxation of the assumption, common to all component separation algorithms developed so far, about the separability between space and frequency dependence for all the signal to recover. In a forthcoming work we'll face how ICA based algorithms for blind component separation deal with maps affected by the most important systematics errors.

ACKNOWLEDGEMENTS

Carlo Baccigalupi warmly thanks Radek Stompor for several useful discussions.

We are also grateful to Giovanna Giardino for providing all sky maps of simulated synchrotron emission (Giardino et al. 2002), which has been named S_G model in this paper.

REFERENCES

Amari S., Chichocki A., 1998, Proc. IEEE 86, 2026

Baccigalupi C., Bedini L., Burigana C., De Zotti G., Farusi A., Maino D., Maris M., Perrotta F., Salerno E., Toffolatti L., Tonazzini A., 2000, MNRAS, 318, 769

Baccigalupi C., Burigana C., Perrotta F., De Zotti G., La Porta L., Maino D., Maris M., Paladini R., 2001, A& A, 372, 8

Baccigalupi C., Balbi A., Matarrese S., Perrotta F., Vittorio N., 2002a, Phys.Rev. D65 063520

Baccigalupi C., De Zotti G., Burigana C., Perrotta F., 2002b, in Astrophysical Polarized Backgrouds, AIP conference proc. 609, S. Cecchini, S. Cortiglioni, R. Sault, and C. Sbarra eds., p. 84

Becker R.H. et al., 2001, AJ, 122, 2850

Burigana C., La Porta L., 2002, in Astrophysical Polarized Backgrouds, AIP conference proc. 609, S. Cecchini, S. Cortiglioni, R. Sault, and C. Sbarra eds., p. 54

Brouw W.N., Spoelstra T.A.T., 1976, A& AS 26, 129

Bouchet F.R., Prunet S., Sethi S.K., 1999, MNRAS, 302, 663

De Bernardis, P. et al., 2002, ApJ 564, 559

De Zotti G., 2002 in Astrophysical Polarized Backgrouds, AIP conference proc. 609, S. Cecchini, S. Cortiglioni, R. Sault, and C. Sbarra eds., p. 295

Duncan A.R., Haynes R.F., Jones K.L., Stewart R.T., 1997, MNRAS 291, 279

Duncan A.R., Reich P., Reich W., Fürst E., 1999, A& A 350, 447

Fosalba P., Lazarian A., Prunet S., Tauber J.A., 2002, in Astrophysical Polarized Backgrouds, AIP conference proc. 609, S. Cecchini, S. Cortiglioni, R. Sault, and C. Sbarra eds., p. 44

Giardino G., Banday A.J., Grski K.M., Bennett K., Jonas J.L., Tauber J., 2002, A& A 387, 82

see Górski K.M., Wandelt B.D., Hansen F.K., Hivon E., Banday A. J., 1999, astro-ph/9905275, and the HEALPix home page <http://www.eso.org/science/healpix/>

Haffner L.M., Reynolds R.J., Tufte S.L., 1999, ApJ, 523, 223

Halverson, N.W. et al. 2002, ApJ 568, 38

Haslam C.G.T. et al., 1982, A&A S 47, 1

Hyvärinen A., 1999, IEEE Signal Processing Lett. 6, 145

Hobson M.P., Jones A.W., Lasenby A.N., Bouchet F., 1998, MNRAS 300, 1

Hu W. 2002, Phys.Rev.D 65, 023003

Hu W., White M., Seljak U., Zaldarriaga M., 1999, Phys.Rev. D57 3290

Kamionkowski M., Kosowsky A., Stebbins A., 1997, Phys.Rev. D55, 7368

Kodama H., Sasaki M., 1984, Progr. Theor. Phys. Suppl. 78, 1

Kogut A., Hinshaw G., 2000, ApJ 543, 530

Lazarian A., Prunet S., 2002, in Astrophysical Polarized Backgrouds, AIP conference proc. 609, S. Cecchini, S. Cortiglioni, R. Sault, and C. Sbarra eds., p. 32

Lee, A.T. et al. 2001, ApJ 506, 485

Maino D., Farusi A., Baccigalupi C., Perrotta F., Banday A. J., Bedini L., Burigana C., De Zotti G., Grski K. M., Salerno, E., 2002, MNRAS, 334, 53

Mandolesi N., et al., 1998, PLANCK Low Frequency Instrument, a proposal submitted to ESA

Liddle A., Lyth D.H. 2000, Cosmological Inflation and Large Scale Structure, Cambridge University Press

Mesa D., Baccigalupi C., De Zotti G., Gregorini L., Mack K.L., Vigotti M., Klein U., submitted to A& A, 2002

Moscardini L., Bartelmann M., Matarrese S., Andreani P., MNRAS in press, 2002

Padin S. et al., 2001, ApJL 549, L1

Puget J. L., et al., 1998, High Frequency Instrument for the PLANCK mission, a proposal submitted to ESA

Schlegel D.J., Finkbeiner D.P. & Davies M., 1998, ApJ 500, 525

Seljak U., Zaldarriaga M., 1996, ApJ 469, 437

Smoot G.F., 1999, in 3K cosmology, AIP conf. proc. 476, L. Maiani, F. Melchiorri, N. Vittorio eds, p. 1

Stolyarov V., Hobson M.P., Ashdown M.A.J., Lasenby A.N., 2002, MNRAS in press

Tegmark M., Efstathiou G., 1996, MNRAS 281, 1297

Tenorio L., Jaffe A. H., Hanany S., Lineweaver C.H., 1999, MNRAS 310, 823

Toffolatti L., Argueso Gomez F., de Zotti G., Mazzei P., Franceschini A., Danese L., Burigana, C., 1998, MNRAS 297, 117

Tucci M., Carretti E., Cecchini S., Fabbri R., Orsini M., Pierpaoli E., 2000, New Astronomy 5, 181

Tucci M., Carretti E., Cecchini S., Nicastro L., Fabbri R., Gaensler B.M., Dickey J.M., McClure-Griffiths N.M., 2002, ApJ in press

Uyaniker B., Fürst E., Reich W., Reich P., Wielebinski R., 1999, A& AS 138, 31

Vielva P., Martínez-González E., Cayón L., Diego J.M., Sanz J.L., Toffolatti L., 2001, MNRAS 326, 181

Wright E.L., 1999, New Astr. Rev. 43, 257

Zaldarriaga M., 2001, Phys.Rev.D 64, 103001

Zaldarriaga M., Seljak U., 1997, Phys.Rev.D 55, 1830